Petroleum and Coal

**Article** **Open Access**

# Pore Pressure and Geomechanical Properties of Reservoir in Miocene Niger Delta Region.

*Jacinta C. Nwosu, Godwill U. Chukwu, Magnus U. Igboekwe, Okechukwu E. Agbasi**

*Michael Okpara University of Agriculture, Umudike, Nigeria*

Received June 17, 2021; Accepted January 14, 2022

**Abstract**

An accurate prediction of pore pressure is very essential in reducing the risk involved in a well or field life cycle. This has formed an integral part of routine work for exploration, development and exploitation team in the oil and gas industries. Several factors such as sediment compaction, overburden, lithology characteristics, hydrocarbon pressure and capillary entry pressure contribute significantly to the cause of overpressure. Hence, understanding the dynamics associated with the above factors will certainly reduce the risk involved in drilling and production. At the background to these challenges is the vague understanding of the subtle complexities that may characterize the geopressure system. Pore pressure and geomechanical properties were estimated in a viable reservoir in the study area. Eaton's pore pressure resistivity is between 1.440 – 1.731 psi/ft, while pore pressures sonic is between 1.440 – 1.601 psi/ft, the overburden pressure range between 3.065 to 3.169 psi/ft. Velocity and Poisson ratio in the reservoirs is between 1.699 – 1.962 and 0.235 – 0.324. The geomechanical analysis was used to infer GOC (Gas-Oil Contact) and OWC (Oil-Water Contact). Reservoir G14 R2, have the highest values pore pressures, due to the fluid content of the reservoir, its more of OWC, with just 66.1% of hydrocarbon in a pore space of 25.8%. The values of pore pressure are seen to correspond to the fluid content delineated from geomechanical evaluation of the reservoirs in the study area.

***Keywords***: *Reservoirs; Compaction; Overburden; Fracture gradient; Fracture pressure.*

## 1. Introduction

Secure, economical and efficient development of reserves of oil and natural gas requires an adequate understanding of the regimes, patterns and distribution of subsurface pressure. Precise prediction of gradients of pore-pressure and fracture within an interest zone becomes a must. Awareness of pore pressure gradient formation and the resulting fracture gradient is one of the criteria for safe drilling. The pressure of the fluid inside the pore spaces of the reservoir rock matrix is pore pressure. It is a function of effective stress formation and overburden stress (the pressure arising from the combined weight of the rock matrix and the fluids in the porous space that are overlying interest formation) [1–2]. If the pore pressure of a formation at any depth for such formation is above the hydrostatic pressure, the pressure is known to be overpressed. On the other hand, the formation is said to be under-pressured when the formation pressure is below the hydrostatic pressure at any depth. The usual pressure for normal geological setting is the hydrostatic pressure, or the pressure exerted by a column of water from the depth of formation to the sea level. As impermeable rocks such as shale sediments are compacted, their pore fluids will not always escape and the total overlying rock column leading to anomalous pressure of formation must then be assisted [3–5].

The numerous pressures of formation experienced in an environment both during the discovery and extraction of the reservoir of hydrocarbon resources play a vital role. The various forms of reservoir pressure commonly experienced during the drilling process are generally divided into three main components: hydrostatic pressure, overload pressure and formation pressure. Vertical pressure is referred to as overload pressure or geostatic pressure at every point on the earth [6–7]. At any level, the overload pressure is a function of the mass of rock

and fluid above the point of interest. The average density of the material (rock and fluids) above the point of interest must be calculated in order to measure the overburden pressure at any time. A formation's pore pressure refers to that portion of the overburden pressure that is not provided by the rock matrix but rather by the liquids that occur in the formation spaces [8]. Compaction, fluid expansion, fluid migration and tectonics [9] are the primary causes of over-pressure. If the pore pressure is lower than usual hydrostatic pressure, the formation is said to be sub-normally under pressure, but if the predicted hydrostatic pressure for that depth is surpassed, the region is considered abnormally under pressure. Identifying the over-pressured drilling zones is important because it narrows the available mud drilling window. Drilling under close mud windows raises the risk of structure fracturing or inviting blow-outs. Proper knowledge of the pressure on the pores will reduce the cost of the well and can help well plan a safe secure drill.

Awareness of a subsurface formation's rocks or fluid characteristics is crucial to the analysis of the oil and gas industry. Hence, understanding the rock formation existence is based on measuring petrophysical parameters such as porosity, saturation and permeability. Unfortunately, uniform and constant-character rock formations are rare. Because of variations in conditions such as strain, temperature, and fluid changes, the relation between petrophysical parameters measured on core samples is often ill-defined. While all of these conditions are considered before drilling, the pressure effect is one significant condition that should not be overlooked [10]. The formation pressure is classified into three categories; normal, abnormal and subnormal formation pressure [11]. The abnormal and sub-normal pressure of formation indicates a pressure higher or lower than this normal condition, respectively. These are induced by various processes such as under-compaction, unloading of the fluid expansion, lateral transfer, etc. As vertical tension rises during the deposition of sediments under compaction, the pore fluid leaks as the pore spaces attempt to compact. If a layer of material with low permeability prevents the escape of pore fluids at a rate sufficient to keep up with the rate of increase in vertical stress, the pore fluid starts to bear a large part of the load and the pore fluid pressure increases [12]. The loading mechanism of fluid expansion occurs when the rock matrix limits the increased volume of the pore fluid resulting from processes such as heating, clay dehydration and hydrocarbon maturation [13], whereas the lateral transfer mechanism occurs when sediments have fluid injected into it from more pressure zone under any given compaction condition. However, as oil/gas exploration spreads to the deeper areas of the planet, this presents a great challenge as it is most likely to experience irregular (higher) pore pressures. These lead to drilling problems such as blowout, kicks, instability in the borehole, stuck shaft, mud lost circulation among others. A pre- and post-drill prediction of pore pressure is therefore important for safe and economical well drilling in overpressured formation and this is the primary aim of this research.

The economics and profitability of such ventures influence significant decisions on projects. Exploration and production of oil and gas resources require well-informed decisions to direct well-planning, logistics drilling, and target opportunities for sustainable development.

For precise analysis of specific subsurface data and characterization of formation, exploration requires geo-pressure information. There are global examples of expensive wells that could not be extracted because only residual hydrocarbons were found to contain the target reservoirs as a result of fluid losses due to fractures initiated by extreme high formation pressures in the bounding seals [14–15]. To properly plan wells and apply the correct drilling mud weights for optimum project delivery, drilling campaigns require accurate estimates of formation pressures. Drilling problems associated with pressure include kicks and inflows, borehole instability, tool sticking, weak drilling fluid returns and sometimes blowouts. As a result, the formation may be affected by an improper drilling program and make the target reservoir inoperable. The quantification and control of pore pressures significantly impacts the prospect from discovery to development and degradation over its entire life-cycle.

## 2. Geologic setting of study area

The Niger Delta Basin, is an extensive rift basin situated on the reactive continental margin near the west coast of Nigeria in the Niger Delta and the Gulf of Guinea, with suspected or confirmed access to Cameroon, Equatorial Guinea, and São Tomé and Príncipe [16–17]. The Niger Delta Basin lies within a wider tectonic structure in the south-westernmost part. It covers an area within longitude $4^0$E - $9^0$E and latitudes $4^0$N - $9^0$N. This basin is very intricate and has a high economic value since it contains a prosperous petroleum system. The filling of sediments has a depth between 9-12 km. It is consisting of several different geological formations indicating how this basin might have developed, as well as the area's regional and large-scale tectonics [18–19]. The Niger Delta Basin is an extensive basin flanked by several other basins in the area all of which were formed by similar structures.

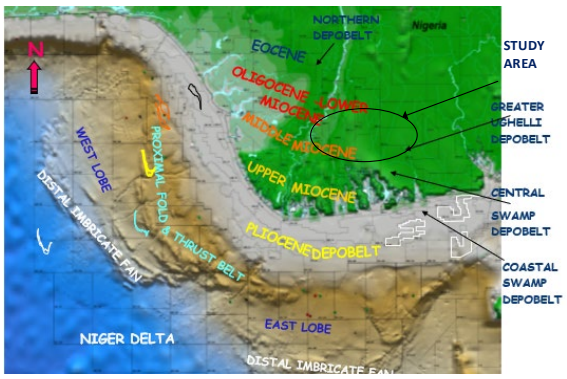


Fig. 1. Geology of the Niger Delta Region

The sedimentary fill of the Niger Delta basin has been subdivided into three (3) broad lithofacies units, which include the marine shales (Akata Formation); marginal marine sandstones, shales and clays (Agbada Formation); and massive continental sandstones (Benin Formation). The Akata Formation is the oldest units and forms the base of the sequence in each depobelt and has stratigraphic thickness which may reach 7000 m in the central part of the delta [20]. Overlying the Akata Formation is the paralic Agbada Formation represented by sands, shales and clays alternations in various proportion and thickness deposited in a number of delta- front, delta-topset and fluvio-deltaic environments. It has a maximum thickness of about 3000 m. The Benin Formation is the youngest unit with variable thickness which becomes thinner offshore [21–22]. This generally regressive clastic sequence of the delta reaches a maximum thickness of about 9-12 km [23].

## 3. Methodology

### 3.1. Materials

Two composite wireline log data including Calliper, Gamma Ray, Resistivity, Neutron, Density and Sonic log from a field in the Niger Delta Region of Nigeria was used for evaluating Petrophysical, Pore Pressure and Geomechanical properties of potential reservoirs in the wells.

### 3.2 .Petrophysical analysis

Normal assessment techniques for formation were used to derive porosity ($\phi$), shale volume, and water saturation (Sw). The flashed zone approach was used to classify hydrocarbon bearing zone within the well-studied reservoir of all. The hydrocarbon bearing zones of the wells were delineated using a combination of GR log and induction resistivity curves. To label clean areas, the GR log was first used. The deep induction log resistivity curve will read a high resistivity in hydrocarbon-bearing areas, since the formation of hydrocarbons is more resistant than saltwater. When the spontaneous potential log is skewed, the Gamma Ray log is especially helpful for identifying shale beds. The GR log represents the percentage of shale and can be used qualitatively as a shale indicator in many areas. At a point halfway between the maximum and minimum deflection of the anomaly, the bed boundary is chosen.

In a Shaly formation, there are various different ways of determining the volume of Shale (Vsh) [24]. The volume of Shale (Vsh) can be calculated in a porous and permeable Shaly zone from the deflections in the GR curve.

$$I_{GR} = \frac{GR_{log} - GR_{min}}{GR_{max} - GR_{min}} \quad (1)$$

$$V_{sh} = 0.08(2^{(3.71IGR)} - 1) \quad (2)$$

Porosity can be calculated from sonic logs using the Wyllie time average in equation

$$\phi = \frac{\Delta t_{log} - \Delta t_{max}}{\Delta t_{ft} - \Delta t_{max}} \quad (3)$$

where: $\Delta t_{log}$ is the reading on the sonic log in μs/ft; $\Delta t_{max}$ is the transit time of the matrix for fresh water).

Using the Archie's equation that related the formation factor (F) to the resistivity of a formation at 100% water saturation ($R_0$) and the resistivity of formation water ($R_w$), the resistivity of the formation water was estimated as a

$$S_w = \left[\frac{aR_w}{a^m R_t}\right] = [a^{1-m}.R_w R_t]^{n-1} \quad (4)$$

where F is formation factor, $S_m{}^n$ is the water saturation of the uninvaded zone, $R_0$ is the resistivity of formation at 100% water saturation and $R_t$ is the true formation resistivity

The Bulk volume of water (BVN) is given by

$$BVW = \phi \times S_w \quad (5)$$

where ϕ is the porosity and $S_w$ is the water saturation.

From water saturation $S_w$, hydrocarbon saturation can be estimated using

$$S_w + S_H = 1 \quad (6)$$

where $S_w$ depicts water saturation and $S_H$ represents hydrocarbon saturation

The main petrophysical parameters needed to evaluate a reservoir then, are its porosity, hydrocarbon saturation, and volume of shale.

### 3.3. Geomechanics

The reciprocal of velocity is the specific acoustic time, which is recorded on the Acoustic log in μsec/ft. The conversion equation between velocity and slowness is given as [25–26]:

$$V_s = \frac{304878}{\Delta T_s} \quad (7)$$

($\Delta T_s$ is in microseconds per foot, and the velocity; $V_s$ is in feet per second).

Another essential elastic constant, named Poisson's ratio, is defined as the strain ratio in a perpendicular direction to the strain in the extensional force direction.

In order to increase distances between neighbouring molecules, from solids to liquids to gases. As a result, solids have no compressibility when compared with liquids and gases. In fact, the bulk modulus is the compressibility reciprocal, and is therefore often referred to as the incompressibility coefficient [27].

The relationship between sonic wave velocities and elastic constants is defined in terms of good logging parameters and in practical units. Is represented the elastic constants

$$\text{Poison's ratio } v = 0.5 \times \frac{\Delta t_s^2 - 2\Delta t_c^2}{\Delta t_s^2 - \Delta t_c^2} \quad (8)$$

where $\Delta t_s$ is compressional wave velocity and $\Delta t_c^2$is shear wave velocity

### 3.4. Pore pressures

The Eaton method is an analytical method used to estimate the acoustic, resistivity, and density log pore pressure that has been calibrated to calculate the pore pressure. This log data will provide an indicator of the overpressure pressure state and usual pressure zone by clique [28–29]. One of the commonly used quantitative methods is the Eaton techniques, such as resistivity plots and sonic plots, which put an empirical formula on a regionally defined exponent. For the measurement of pore pressure gradients by resistivity, Eaton used the following equation:

$$PP = OBG - (OBG - PP_N)(R_o/R_N)^X \quad (9)$$

where PP is the pore pressure gradient (ppg); OBG is the overburden gradient (ppg); $PP_N$ regarded as the normal pore pressure gradient (ppg); $R_O$ is the observed resistivity (ohm-m); $R_N$ is the normal resistivity (ohm-m) and x is the Eaton exponent which is 1.2.

In Eaton's above equation it is very difficult to determine the hydrostatic pore pressure shale resistivity state, the best way out is to determine the hydrostatic pore pressure shale resistivity state, the best way out is to determine the normal compaction trendline for the prediction of pore pressure, since the normal resistivity RN is a function of burial depth [30–31].

This equation of the usual compaction trend of resistivity can, however, be used as such because of the relationship of restrained resistivity and burial depth in normal pressure formation:

$$lnR_N = lnR_o + bZ \quad (10)$$

where $R_N$ is the shale resistivity in the normal compaction states; $R_O$ is the shale resistivity in a mudline; b is the constant while Z is the depth of the mud line below.

By substituting eq. 9 into eq. 10, Eaton's resistivity equation can be written as followings:

$$P_{pg} = OBG - (OBG - P_{ng})(R/R_o\, e^{bz})^n \quad (11)$$

where R is the shale resistivity measured at depth Z; $R_O$ is the normal compaction shale resistivity in the mudline and b is the logarithmic resistivity normal compaction line slope.

Eaton [32] presented an empirical equation used for pore pressure gradient prediction from sonic compressional transit time ($\Delta t_n$) based on:

$$P_{pg} = OBG - (OBG - P_{ng})(\Delta t_n/\Delta t)^3 \quad (12)$$

where $\Delta t_n$ is the sonic transit time or the slowness in shale at normal pressure.

Sayer, [12] worked on Eaton [33] relationship as follow:

$$V = V_o + Kz \quad (13)$$

where V is the seismic velocity at the depth Z and $V_o$ is the ground surface velocity; k is a constant, as a normally pressure velocity for pore pressure prediction.

The overburden gradient was calculated by measuring the volume of bulk density of shale from the gamma ray log relative to the Kelly height and water depth to determine the compressibility rate of the selected wells, i.e. the effective stress due to the fact that porous rocks are subjected to internal and external stress when buried, internal stresses emerge from the fluid pore pressure with typing, this combination of the external and internal stress resulted in the reservoir having a resulting strain or rock deformation.

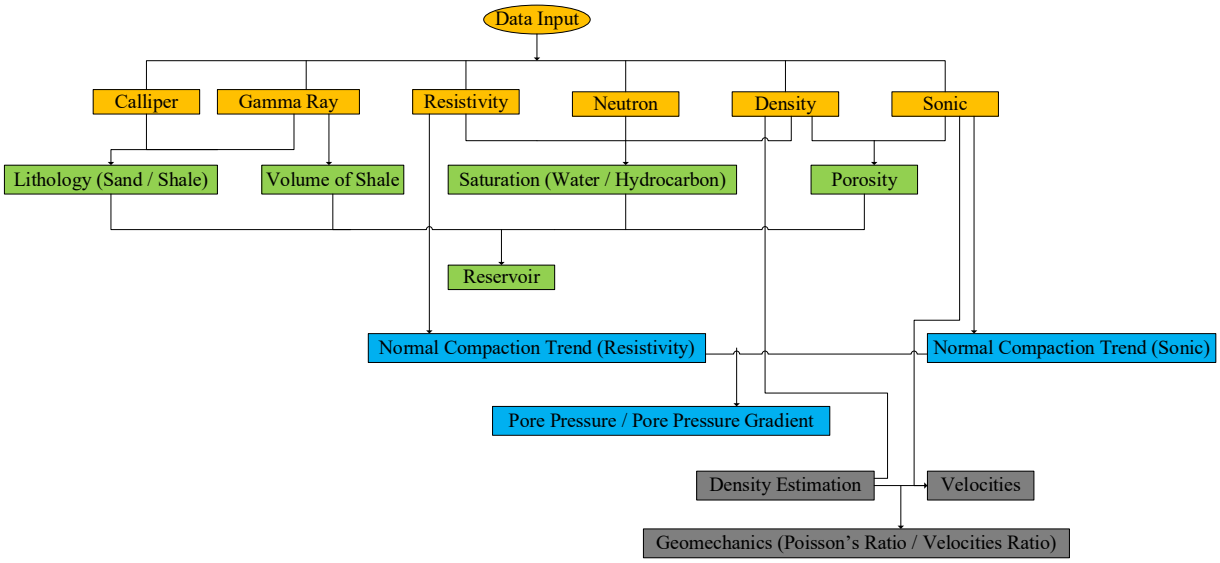


Fig. 2. Flowchart for petrophysics, pore pressure and geomechanical analysis

## 4. Results and discussions

Petrophysical and pore pressure analysis for the two wells are presented in Figures 3 and 4, were two reservoirs were identified in each well. The reservoirs were delineated based on low gamma ray values for sand, a cross over log of density and neutron with density to the left and neutron to the right and with high resistivity values. Porosity, volume of shale and water saturation was then evaluated for the zones. The reservoirs are all economical viable with porosity between 0.252 to 0.297; volume of shale between 0.024 to 0.195; water saturation between 0.171 to 0.339 (hydrocarbon saturation between 0.661 to 0.829) and net pay zone between 7.468 to 31.852m.

Generally, in the two wells, the porosity values where seen to decrease with depth, the porosities have an inverse relationship with the volume of shale in the reservoirs. The bulk volume of water which is the product of porosity and water saturation gives an idea of how much water would be contained in a pore space per volume of the formation. In the reservoirs the bulk volume of water is between 4.6% to 8.2%, which infers that the other parts between 91.8% to 95.4% is the bulk volume of hydrocarbon.

The depth of the reservoirs is 2416. 302 – 2448.001 m, 2501.646 – 2509.646 m, 3693.566 – 3700.882 m, and 3798.265 – 3812.896 m respectively for well G14 R1, G14 R2, G52 R1 and G52 R2. Tables 1 and 2 show the minimum, maximum and mean values of the petrophysical properties of the reservoirs in the two wells.

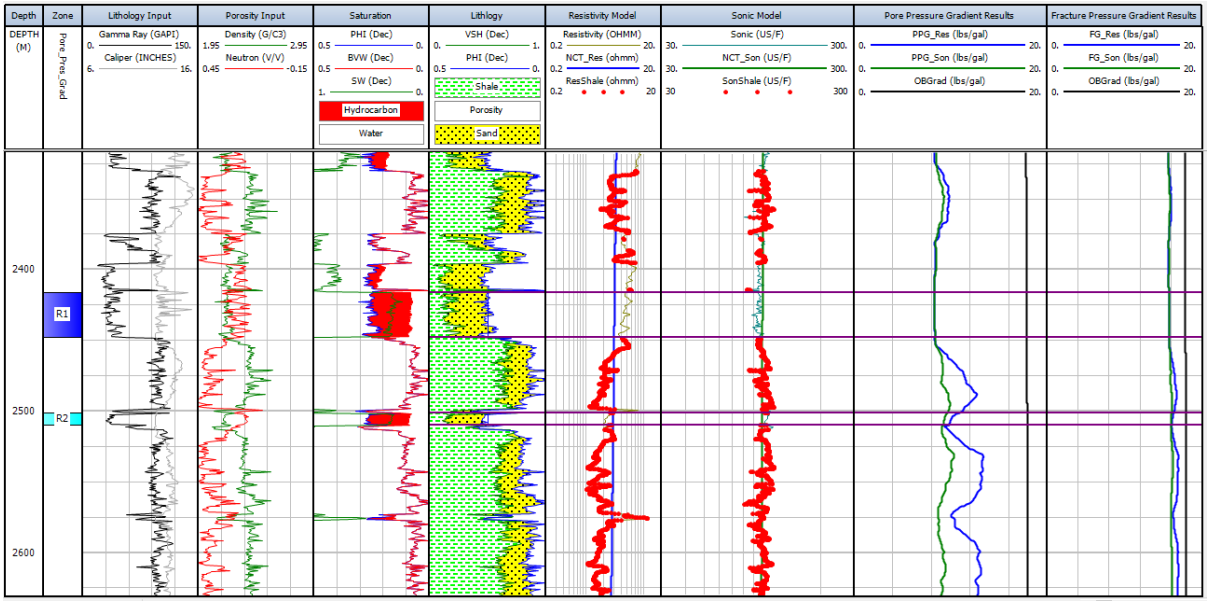


Fig. 3. Petrophysical and Pore pressure plot for Reservoirs R1 and R2 in well G14

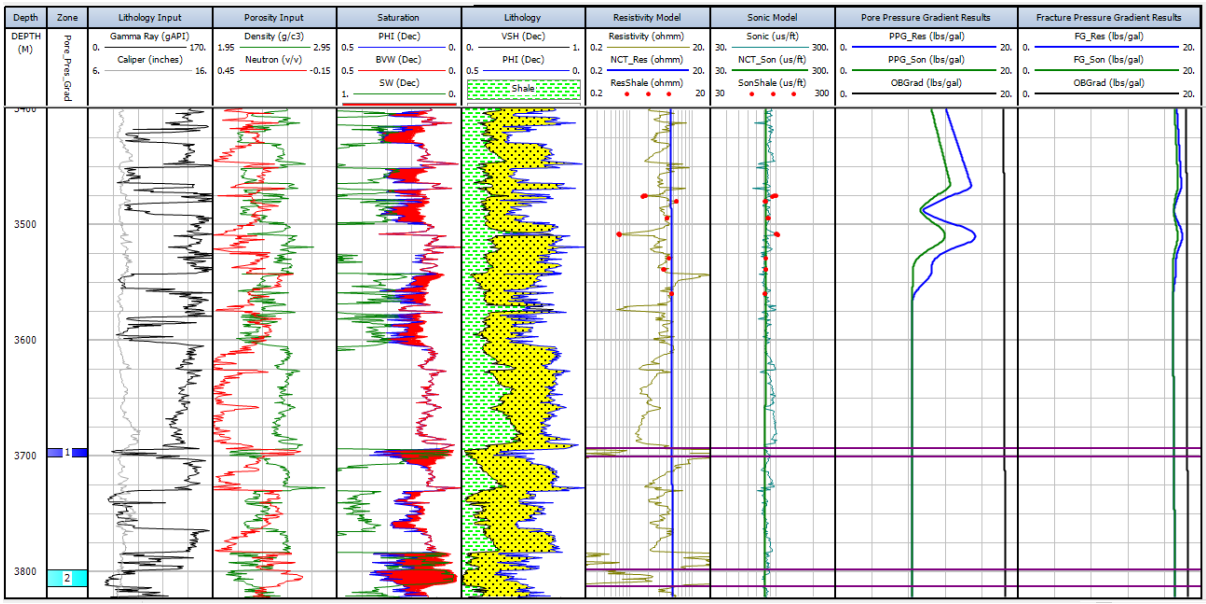


Fig. 4. Petrophysical and Pore pressure plot for Reservoirs R1 and R2 in well G52

Table 1. Petrophysical, Pore pressure and Geomechanical properties of reservoirs R1 and R2 in well G14

| Curve | Units | Top: 2416.302m, Bottom: 2448.001, Net: 31.852 | | | Top: 2501.646m, Bottom: 2509.646m, Net: 8.382m | | |
|---|---|---|---|---|---|---|---|
| | | Min | Max | Mean | Min | Max | Mean |
| PHI | Dec | 0.190 | 0.336 | 0.252 | 0.169 | 0.286 | 0.258 |
| BVW | Dec | 0.070 | 0.093 | 0.082 | 0.077 | 0.093 | 0.087 |
| SW | Dec | 0.218 | 0.457 | 0.327 | 0.306 | 0.484 | 0.339 |
| VSH | Dec | 0.063 | 0.311 | 0.174 | 0.113 | 0.599 | 0.195 |
| NCT_Res | ohmm | 3.050 | 3.112 | 3.081 | 2.933 | 2.949 | 2.941 |
| NCT_Son | US/F | 100.217 | 100.420 | 100.319 | 99.821 | 99.873 | 99.847 |
| PP_Res | psi | 3453.860 | 3549.651 | 3479.808 | 4228.900 | 4504.589 | 4331.287 |
| PP_Son | psi | 3454.081 | 3532.247 | 3480.185 | 3966.375 | 4079.649 | 4016.767 |
| PPG_Res | lbs/gal | 8.345 | 8.466 | 8.354 | 9.839 | 10.515 | 10.094 |
| PPG_Son | lbs/gal | 8.346 | 8.425 | 8.354 | 9.228 | 9.523 | 9.361 |
| FG_Res | lbs/gal | 15.727 | 15.780 | 15.742 | 16.153 | 16.297 | 16.207 |
| FG_Son | lbs/gal | 15.727 | 15.770 | 15.742 | 16.019 | 16.079 | 16.046 |
| FP_Res | psi | 6508.909 | 6615.816 | 6557.402 | 6942.512 | 6981.615 | 6954.434 |
| FP_Son | psi | 6508.958 | 6611.926 | 6557.487 | 6883.692 | 6888.204 | 6885.376 |
| OBGrad | lbs/gal | 17.879 | 17.884 | 17.881 | 17.926 | 17.927 | 17.926 |
| OBPres | psi | 7399.295 | 7498.333 | 7448.764 | 7679.553 | 7705.084 | 7692.315 |
| Pois Ratio | | 0.276 | 0.316 | 0.298 | 0.302 | 0.335 | 0.324 |
| $V_pV_s$ Ratio | | 1.797 | 1.928 | 1.865 | 1.878 | 2.010 | 1.962 |

Table 2. Petrophysical, Pore pressure and Geomechanical properties of reservoirs R1 and R2 in well G52

| Curve | Units | Top: 3693.566m, Bottom: 3700.882, Net: 7.468m | | | Top: 3798.265m, Bottom: 3812.896m, Net: 22.736m | | |
|---|---|---|---|---|---|---|---|
| | | Min | Max | Mean | Min | Max | Mean |
| PHI | Dec | 0.125 | 0.371 | 0.291 | 0.216 | 0.371 | 0.297 |
| BVW | Dec | 0.027 | 0.122 | 0.058 | 0.019 | 0.136 | 0.046 |
| SW | Dec | 0.093 | 0.980 | 0.235 | 0.056 | 0.620 | 0.171 |
| VSH | Dec | 0.014 | 0.142 | 0.053 | 0.000 | 0.159 | 0.024 |
| NCT_Res | ohmm | 4.783 | 4.788 | 4.785 | 4.855 | 4.866 | 4.860 |
| NCT_Son | us/ft | 81.868 | 81.886 | 81.877 | 81.600 | 81.635 | 81.618 |
| PP_Res | psi | 5253.490 | 5263.895 | 5258.692 | 5402.407 | 5423.216 | 5412.812 |
| PP_Son | psi | 5253.490 | 5263.895 | 5258.692 | 5402.407 | 5423.216 | 5412.812 |
| PPG_Res | lbs/gal | 8.345 | 8.345 | 8.345 | 8.345 | 8.345 | 8.345 |
| PPG_Son | lbs/gal | 8.345 | 8.345 | 8.345 | 8.345 | 8.345 | 8.345 |
| OBGrad | lbs/gal | 18.513 | 18.515 | 18.514 | 18.554 | 18.560 | 18.557 |
| OBPres | psi | 11653.803 | 11678.706 | 11666.288 | 12011.002 | 12061.283 | 12036.039 |
| FG_Res | lbs/gal | 17.042 | 17.049 | 17.046 | 17.140 | 17.154 | 17.147 |
| FG_Son | lbs/gal | 17.042 | 17.049 | 17.046 | 17.140 | 17.154 | 17.147 |
| FP_Res | psi | 10728.244 | 10753.802 | 10741.052 | 11095.552 | 11147.342 | 11121.354 |
| FP_Son | psi | 10728.244 | 10753.802 | 10741.052 | 11095.552 | 11147.342 | 11121.354 |
| Pois Ratio | | 0.242 | 0.285 | 0.265 | 0.235 | 0.280 | 0.255 |
| $V_pV_s$ Ratio | | 1.714 | 1.824 | 1.770 | 1.699 | 1.810 | 1.745 |

Figures 5 and 6 show the pore pressure, pore pressure gradient, fracture pressure and fracture pressure gradient estimated from Eaton's equations for sonic and resistivity in the two wells under study. The pressure plots generally show decrease with depth expect in cases with overpressure or under pressure zones in the wells. The pore pressure in psi unit for the reservoirs is between 3479.808 – 5412.812 psi and 3480.185 – 5412.812 psi for Eaton's pore pressure evaluated from resistivity and sonic respectively. The pore pressure (Eaton's pore pressure for resistivity and sonic) shows an increase with depth until approximately 1650 m and 3246 m in well G14 and G52 as seen in figures 5a and 6a respectively, with same effect in pore pressure fracture as seen in figure 5b and 6b. The shales in between the sands seems to be acting as a seal so the reservoir may be challenging independently by production effect. The pore pressure resistivity for well G14 is 3479.808 psi (1.440 – 1.422 psi/m) and 4331.287 psi (1.731 – 1.726) while for pore pressure sonic is 3480.185 psi (1.440 – 1.422 psi/m) and 4016.767 psi (1.606 – 1.601 psi/m) for reservoir R1 and R2 respectively. The pore pressure resistivity for well G52 is 5258.692 psi (1.424 – 1.421 psi/m) and 5412.812 psi (1.425 – 1.420 psi/m) while for pore pressure sonic G52 is 5258.692 psi (1.424 – 1.421 psi/m) and 5412.812 psi (1.425 – 1.420 psi/m). The overburden pressure for G14 is between 7448.764 psi (3.083 – 3.043 psi/m), 7692.315 psi (3.075 – 3.065 psi/m), 11666.288 psi (3.159 – 3.152 psi/m) and 12036.039 psi (3.169 3.157 psi/m) for wells G14 reservoirs R1; R2 and G52 reservoirs R1; R2 respectively. The estimated pre pressure resistivity was seen to vary with the with pore pressure from sonic in the reservoirs in well G14, but it's the same in reservoirs in G52. The variation in the estimated pore pressure in well G14 and G52 reservoirs is due to fluid type that exits in the reservoirs, which points to the fact that using only resistivity to delineate fluid type is not recommended without other log (density-neutron-sonic) as seen inf figures 3 and 4.

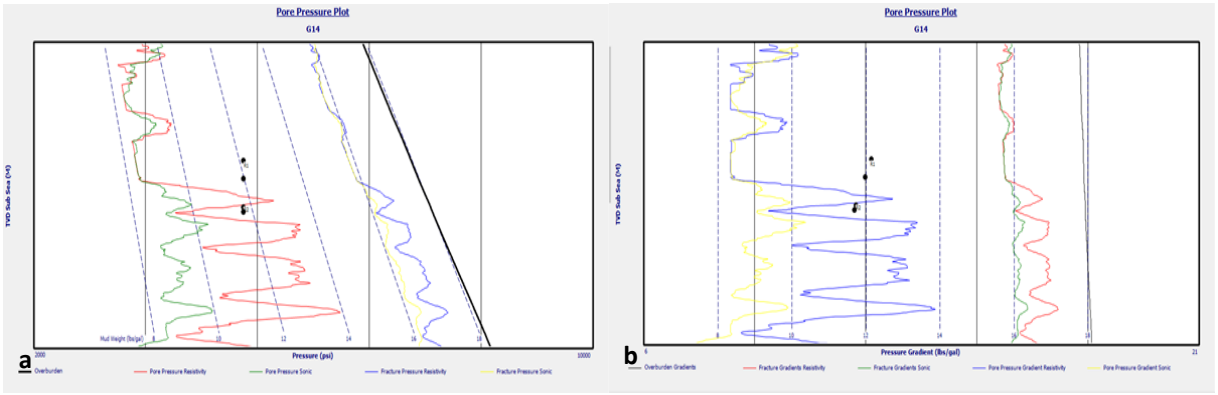


Fig. 5. Pore pressure and pore pressure gradient plot for well G14

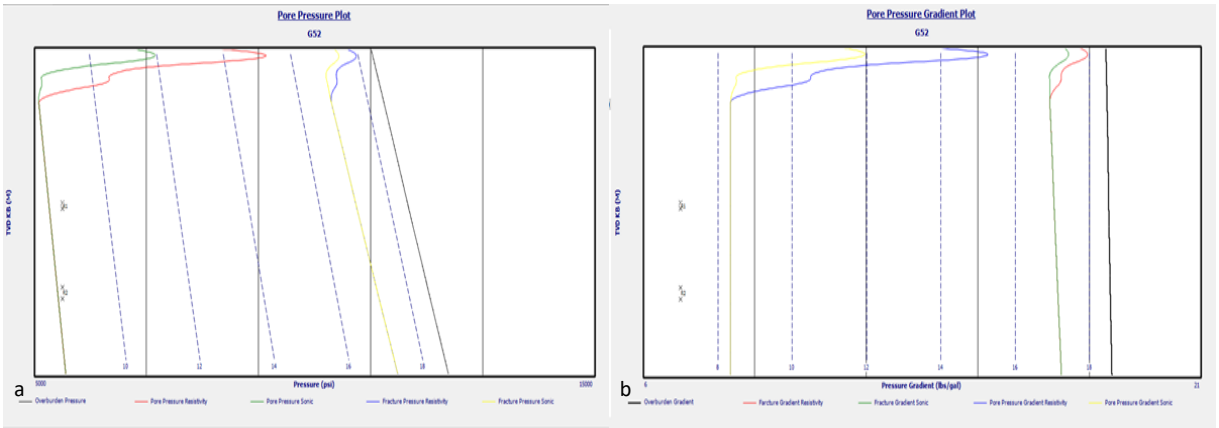


Fig. 6. (a) Pore pressure and (b) pore pressure gradient plot for well G52

The calculated fracture pressure conforms with the pore pressure in each of the reservoirs in well G14 and G52. The range of the fracture pressure is between 6557.487 – 7692.315 psi and 11121.354 – 12036.039 psi for well G14 and G52 respectively.

Density-sonic crossplot with gamma ray (Figure 7a and 8a) for the reservoirs in the wells under study shows in well G14 are clean sands with low values of sonic corresponding to high density values, while well G52 reservoirs are dirty sand with low values of sonic corresponding to high density values. Figure 7b and 8b are crossplot of resistivity and depth with gamma ray, it shows the influence of lithology with fluid types.

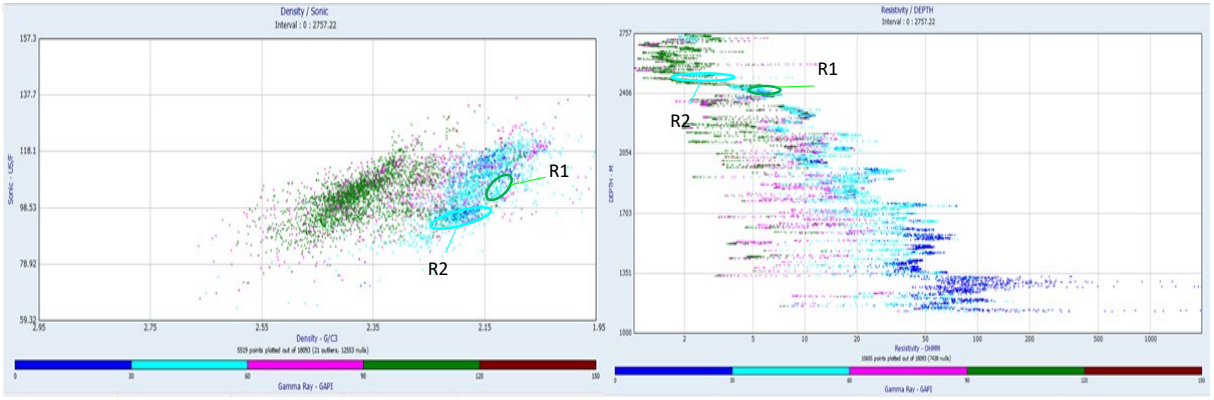


Fig. 7. Density-Sonic crossplot and Resistivity-Depth crossplot with gamma ray for well G14

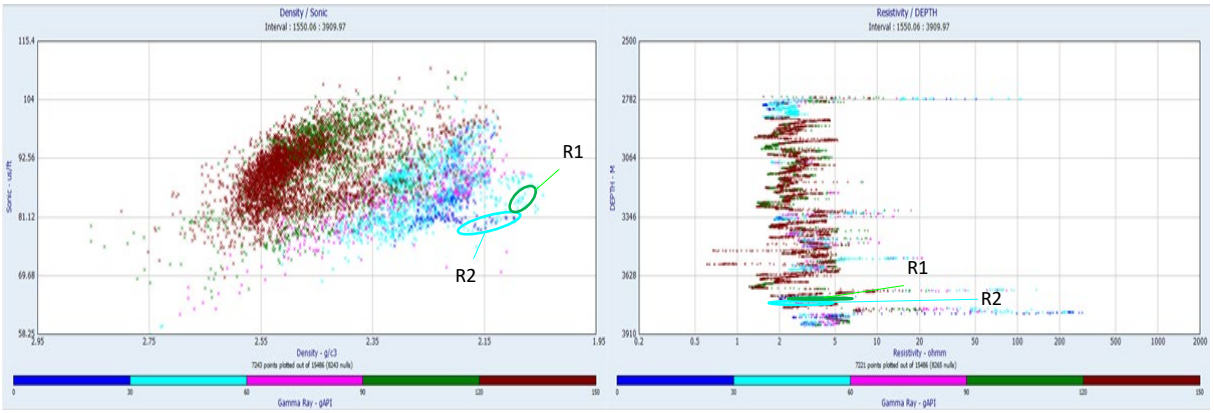


Fig. 8. Density-Sonic crossplot and Resistivity-Depth crossplot with gamma ray for well G52

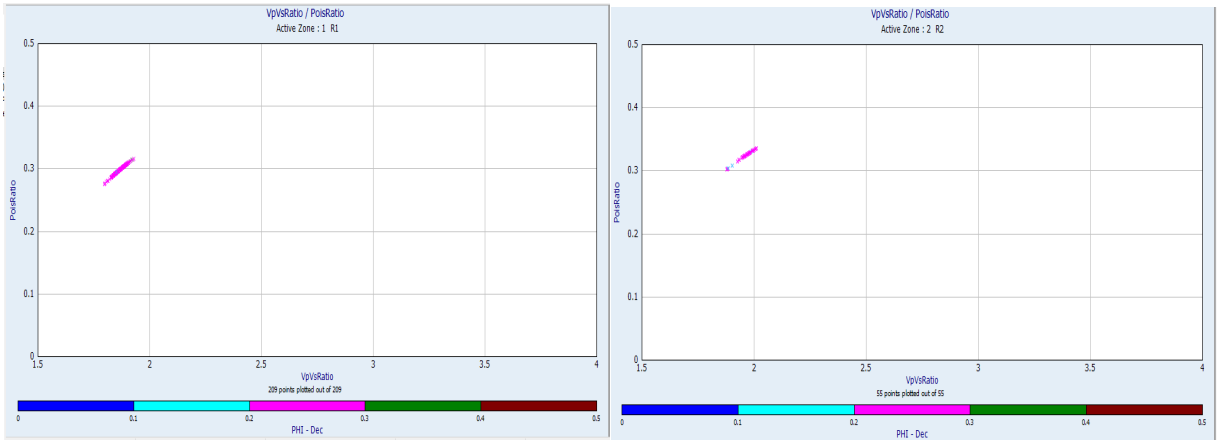


Fig. 9. $V_pV_s$ Ratio-Poisson Ratio crossplot with porosity for reservoir R1 and R2 in well G14

Figures 9 and 10 shows the geomechanics analysis for the reservoirs from Castagna *et al.*,[26] crossplot of $V_pV_s$ Ratio – Poisson Ratio. The crossplot shows that G14 reservoirs are OWC (Oil-Water Contact) while G52 reservoirs are GOC (Gas-Oil Contact). The values of Poisson ratio and $V_pV_s$ Ratio for G14 is between 0.298 – 0.324, while for G52 is between 0.255 – 0.265 and 1.745 – 1.770 as seen in tables 1 and 2. Figures 9 and 10 also shows the porosity in the z-axis, with the reservoirs in G14 been more porous than the reservoirs in G52.

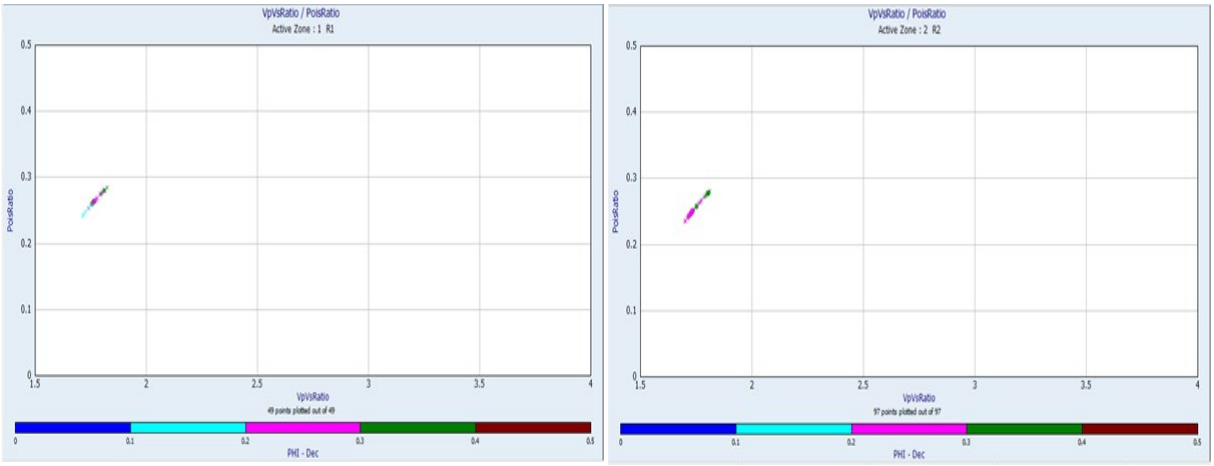


Fig. 10. $V_pV_s$ Ratio-Poisson Ratio crossplot with porosity for reservoir R1 and R2 in well G52

## 5. Conclusion

The Pore pressure model reveals that high pressure zones are marked with high sedimentation rates and deviation from the normal trend of petrophysical properties. The results of this study form the basis for developing an accurate and robust pore pressure prediction strategy and can be applied to other sedimentary basins in predicting over pressures.

Analysis of sonic and density log data shows that overpressure in the field could be inferred to have been generated by disequilibrium compaction of the lower Agbada Formation. Pore fluid prediction is possible by analysing the relationship existing between Poisson's ratio and velocity ratio. From the interpretation guide, it can be observed that gas and oil sand have lower Poisson's and velocity ratio compared to brine sand and shale. The velocity ratio was used not only to deduce lithology but also to detect the presence of hydrocarbons in pores. Velocity ratio is very sensitive to pore fluid of sedimentary rocks. In an oil layer, compressional wave velocity decreases as shear wave velocity increases.

### References

[1] Bell DW. Velocity Estimation for Pore- Pressure Prediction. In Huffman AR; Bowers, GL (ed) Pressure regimes in sedimentary basins and their prediction: AAPG Memoir, 2002; 76, 177–215.

[2] Bowers GL. Pore pressure estimation from velocity data: accounting for overpressure mechanisms besides under compaction. Society of Petroleum Engineers, Drilling and completion, 1995. 89-95.

[3] Golyan MF. Compaction, rock property evolution and rock physics diagnostics of Askeladd discovery, Norwegian Barents Sea; Master Thesis (Masteroppgave). 2012. 50-58.

[4] Huffman AR. Recent advances in pore pressure prediction in complex geologic environment. Society of Petroleum Engineers Paper, Bahrain. 2011.

[5] Corredor F, Shaw JH, and Bilotti F., Structural styles in the deep-water fold and thrust belts of the Niger Delta. AAPG Bulletin, 2005; 89: 753-780.

[6] Anakwuba EK, Onwuemesi AG, Ajaegwu NE, Akpunonu EO, and Onuba .N., Sequence stratigraphic approach in hydrocarbon exploration of Diok Field, Eastern Niger Delta. Natural and Applied Sciences Journal, 2008; 9(1): 41-50.

[7] Onwuemesi AG, and Egboka BCE. Petroleum pro- spects of the Anambra Basin. Natural and Applied Sciences Journal, 2007; 8, (1): 1-7.

[8] O'Connor SA, Swarbrick RE, Hoesni MJ, and Lahann R. Deep pore pressure prediction in challenging areas, Malay Basin, SE Asia, Proceedings of Indonesia Petroleum Association, 35 Annual Convention and Exhibition. 2011.
[9] Zhang J., Pore pressure prediction from well logs: Methods, modifications, and new approaches. Earth Science Reviews; 2011, 108: 50-63.
[10] Amonpantang P. An overpressure investigation by sonic log and seismic data in Morgot Field, Gulf of Thailand: Bulletin of earth sciences of Thailand, 2010; 3(2): 37-40.
[11] Lopez J and Rappold PM, Wieseneck 3D pressure prediction integration of geophysical, geological and petrophysical data and analysis. 2001.
[12] Sayer CM. An introduction to velocity based pore pressure estimate; Schlumberger Data and consulting services, Houston, U.S.A. The Leading Edge, 2006; 25(12): 1496–1500.
[13] Dutta NC. Deep water geohazard prediction using Pre- stack inversion of large offset P wave data and rock model: Western Geco, Houston Texas, U.S. The Leading Edge, 2002; 193-198.
[14] Bowers GL. Detecting high overpressure. Applied Mechanics Technologies, Houston, Texas, U.S. The leading Edge, 2002; 174 - 177.
[15] Brown A. Improved interpretation of wireline pressure data. AAPG Bulletin, 2003; 87(2): 295 – 311.
[16] Tuttle, M.L.W., Brownfield, M.E., and Charpentier, R.R., Tertiary Niger Delta (Akata-Agbada) petroleum System (No. 701901), Niger Delta province. Cameroon, and Equatorial Guinea, Africa: U.S. Geological Survey Open File report 99-50H, 1990.1 - 13.
[17] Agbasi OE, Igboekwe MU, Chukwu GU, and Sunday EE. Discrimination of pore fluid and lithology of a well in X Field, Niger Delta, Nigeria. Arabian Journal of Geosciences, 2018, 11, 274.
[18] Weber KJ, and Daukoru EM. Petroleum geology of the Niger Delta. Proceedings of World Petroleum Congress. Tokyo 2 (Geology), 1975; 209 -221.
[19] Inyang NJ, Akpabio OI, and Agbasi OE. Shale Volume and Permeability of the Miocene Unconsolidated Turbidite Sand of Bonga Oil Field, Niger Delta, Nigeria. International Journal of Advanced Geoscience, 2017; 5(1): 37-45.
[20] Short KC, and Stauble AJ. Outline of Geology of Niger Delta. American Association of Petroleum Geologists Bulletin, 1967; 51: 761 - 779.
[21] Doust H, and Omatsola E. Niger Delta. In: Edwards JD, Santogrossi PA (eds.) Divergent/passive margin basins. AAPG Memoir, 1990; 48: 239 - 248.
[22] Ejedawe J. Nigeria Potential Waiting to be Tapped. AAPG Explorer, May 2012.
[23] Koledoye AB, Aydin AA, and May E. Three-dimensional visualization of normal faults segmentation and its implication for faults growth. The Leading Edge, 2000; 19(7): 692-701.
[24] Aniwetalu EU, and Anakwuba EK. Quantitative Characterisation of Groundroll (Rayleigh Waves) in the Western Niger Delta, Nigeria. Archives of Applied Science Research, 2015; 4: 7-22.
[25] Ungerer PJ, Burrus B, Doligez P, Chenet Y, and Bessis F. Basin Evaluation by integrated two-dimensional modeling of heat transfer, fluid flow, hydrocarbon generation and migration. Am Assoc. Petrol. Geol. Bull., 1990; 74: 309 – 355.
[26] Castagna, J.P., Batzle, M.L., Eastwood, R.L., Relationships between compressional wave and shear wave Velocities in Clastic Silicate Rocks. Geophysics. 1985, 50(4), 571-581.
[27] Chukwuma M, Brunel C, Cornu T, and Carre G. Overcoming pressure limitations in Niger Delta Basin: Digging Deep into New Frontier on Block- X. Journal of Geology and Geosciences, 2013; 2: 112.
[28] Gutierrez MA, Braunsdort NR, and Couzens BA. Calibration and ranking of pore-pressure prediction Shell International Exploration and Production, Houston, USA. The Leading Edge, 2006; 1516-1523.
[29] Hantschel T, and Kauerauf AI. Fundamentals of Basin Modeling, Springer Verlag, Berlin, Germany, 2009, 476
[30] Swarbrick R, O'Connor S, and Lahann R. Maximizing Geological Information from pressure tests and depth plots. Oil and Gas Journal, 2005; (36): 103.
[31] Engelder T. Stress Regimes in the Lithosphere. Princeton University Press. 1993.
[32] Eaton BA. The equation for Geopressure Prediction from well logs, Paper 5544, Society of Petroleum Engineers, Texas. 1975.
[33] Eaton BA. Graphical method predicts geopressures worldwide: World Oil, 1972; 182: 51–56.

*To whom correspondence should be addressed: Okechukwu E. Agbasi, Michael Okpara University of Agriculture, Umudike, Nigeria, E-mail: agbasi.okechukwu@gmail.com*